

Whistler Wave Mode Conversion to Lower Hybrid Waves at a Density Striation

J. F. Bamber, W. Gekelman, and J. E. Maggs

*Department of Physics, University of California at Los Angeles, 1000 Veteran Avenue, Room 15-70,
Los Angeles, California 90024-1696*

(Received 1 August 1994)

The first observation of mode conversion of whistler waves to lower hybrid waves at a density striation has been made in a laboratory plasma. The observed lower hybrid wavelength is consistent with that predicted by linear mode coupling. The lower hybrid waves have amplitudes up to 20% of the incident whistler waves.

PACS numbers: 52.35.Hr

It has been believed for a number of years that electromagnetic whistler waves, either artificially launched or naturally produced by lightning, propagating in regions of the ionosphere containing field-aligned density striations, could interact with these striations to produce electrostatic lower hybrid waves. Several key experiments performed in the ionosphere have yielded strong evidence for mode conversion in conjunction with density striations. In particular, Bell and Ngo [1] have shown that whistler waves launched from ground-based transmitters stimulate lower hybrid waves as they propagate through the auroral and subauroral ionosphere. The presence of plasma density irregularities in these regions has been established [2]. These authors also present a simple theoretical model in which whistler waves reflect from a sharp planar interface between regions of different plasma density. This model is very useful in understanding basic properties of the interaction.

Our goal was to perform, in a controlled laboratory experiment, a detailed study of the interaction of whistler waves with a single field-aligned density striation in parameter regimes directly applicable to the ionospheric interaction. In the laboratory experiment, the parallel wave number k_{\parallel} is provided by the incident whistler wave, and a broad spectrum of perpendicular wave numbers k_{\perp} is provided by the striation. For frequencies between the lower hybrid resonance and half the electron cyclotron frequency, $f_{LH} < f < f_{ce}/2$, the cold plasma dispersion relation allows up to four values of k_{\perp} for any k_{\parallel} corresponding to a whistler wave. Thus, the incident

wave potentially can linearly couple to four new wave modes: one whistler and one lower hybrid mode inside, and one whistler and one lower hybrid mode outside, the striation.

A schematic diagram of our experiment is shown in Fig. 1. The work is carried out in the LAPD (Large Plasma Device) at UCLA [3]. A dc discharge plasma is produced using an oxide coated cathode. A plasma column 70 cm in diameter is formed in the main region of the plasma chamber where the magnetic field strength $|\mathbf{B}_0|$ is 540 G. By leaving a small region in the center of the cathode uncoated, a striation of lower density plasma is created along the center of the plasma column with a diameter d of ~ 4 cm. The density in the main part of the plasma for this experiment is $1.1 \times 10^{12} \text{ cm}^{-3}$ and in the striation $4.0 \times 10^{11} \text{ cm}^{-3}$. (The plasma density is measured using a Langmuir probe and is calibrated by matching the whistler wave radiation pattern in a uniform region of the plasma to a radiation pattern calculated using a Green's function analysis of our loop antenna in a uniform plasma.) The density gradient scale length at the edge of the striation L_{∇} is 1.7 cm. A 2 cm diameter magnetic loop antenna is inserted into the plasma, 11 cm from the striation, oriented with its normal parallel to \mathbf{B}_0 . The loop is completely insulated from the plasma in order to ensure purely inductive coupling. The size and inductive nature of the antenna results, almost exclusively, in radiation in the whistler wave mode, with less than 0.1% of the radiated energy going into the lower hybrid mode. A 101 MHz signal is applied to the antenna in

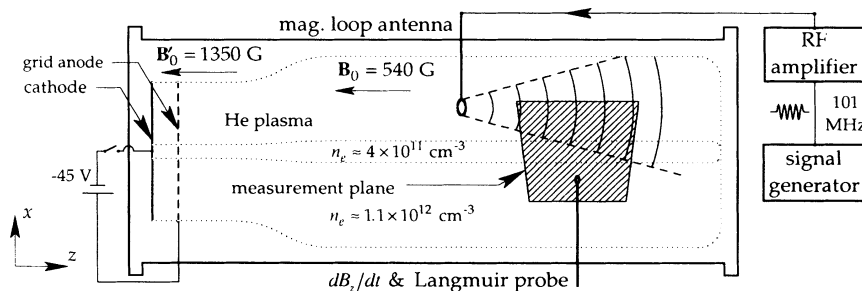


FIG. 1. Schematic drawing of the experimental setup.

TABLE I. Comparison of parameter ratios in the LAPD and the ionosphere.

Ratio	LAPD	Ionosphere (~ 10 km)
f/f_{LH}	5.6	1–6
f/f_{ce}	0.067	0.005–0.030
f_{pe}/f_{ce}	6.3	0.6–1.0
d/r_{ci}	12	20
d/L_{∇}	2.6	10
λ_{\parallel}/d	4	5–60
$\lambda_{\perp,LH}/d$	0.31	2–3
$\lambda_{\parallel}/\lambda_{\perp,LH}$	13	20–300

a very long pulse containing over 1000 wave periods. All of the parameters discussed above (magnetic field strength, plasma density, wave frequency, and striation diameter) are chosen so that the calculated wavelength and scale length ratios are as close as possible to those typically observed in the ionosphere. Ratios of relevant physical quantities in the laboratory plasma are compared to those in the ionosphere in Table I. It is seen that the majority of the LAPD experimental conditions scale so as to lie within the ranges observed in the ionosphere.

Data are taken near the end of the wave pulse under steady state conditions. They are sampled with a 1 ns resolution for over 30 wave periods. The relative phase of this signal to the input signal is calculated with an accuracy of $\sim 5\%$, the uncertainty arising from shot to shot noise in the plasma. Spatially, measurements are made in a planar grid through the center of the striation as shown in Fig. 1. The axial location of the center of the data plane is near the region where radiation from the antenna first impinges upon the striation. The origin of the coordinate system used for displaying data is taken to be at the center

of the antenna; thus, the coordinates of the measurement region extend from $z = 21$ cm to $z = 43$ cm and from $x = -19$ cm to $x = -2$ cm at $y = 5$ cm. Parallel to \mathbf{B}_0 , the spacing between data points Δz is approximately 1 cm (varying with x); in the perpendicular direction $\Delta x = 0.1$ cm in order to resolve the short wavelength lower hybrid waves. The accuracy of the spacing of the grid points is 0.03 mm. Note that the plane begins over one parallel wavelength away from the antenna and is centered, in x , on the striation. A single-turn, 3 mm diameter induction loop is used to measure the wave fields. The diameter of the wire forming the loop (0.3 mm) and the diameter of the shaft (0.9 mm) are both small compared to the ion gyroradius (4.2 mm) and the wavelengths involved (see below). Although lower hybrid waves are often regarded as electrostatic, this is only true for the case of \mathbf{k}_{LH} being exactly at the resonance cone angle. For our experimental conditions $\sim 20\%$ of the energy density of the lower hybrid wave comes from the magnetic field components and, therefore, lower hybrid waves are detectable using a magnetic field probe.

The wave magnetic field data are shown in Fig. 2. The picture on the left, Fig. 2(b), displays the unfiltered data; the picture on the right, Fig. 2(c), shows the data with long perpendicular wavelength components filtered out. The wave magnetic field parallel component $B'_z(x, z)$ is measured. We subsequently scale the $B'_z(x, z)$ data to values which we would obtain if all the energy went into the B_z component of the wave, normalizing so that the unfiltered data range from -1 to 1 and denote these energy-scaled, normalized data $\tilde{B}_z(x, z)$. Energy scaling is necessary in order to make a direct comparison of the two wave modes as a much smaller fraction of the wave energy goes into B_z for the lower hybrid mode. The scale

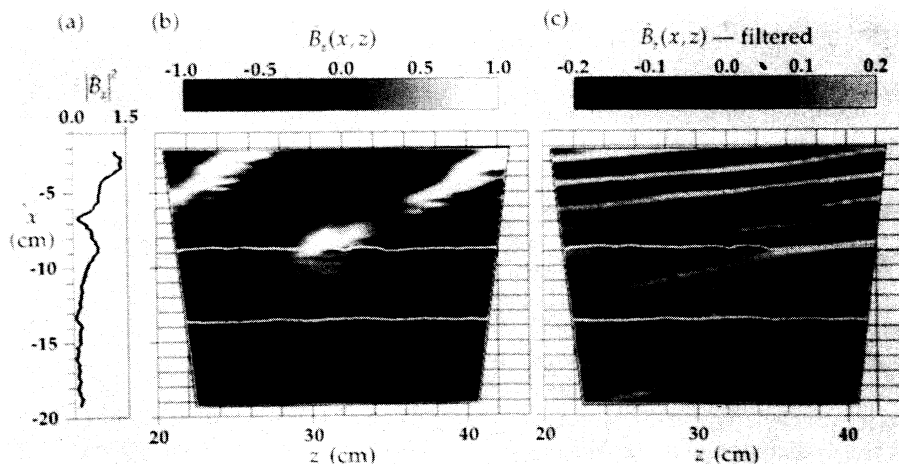


FIG. 2. Energy-scaled, normalized magnetic field data \tilde{B}_z plotted as a function of x and z with lines indicating the striation edges superimposed in (b) and (c). Whistler waves are clearly seen in the unfiltered data (b); lower hybrid waves are revealed by filtering the long perpendicular wavelengths from the data in (c). An amplitude profile of the unfiltered data at $z \approx 32$ cm appears in (a), showing a peak at the edge of the striation.

factor s is

$$s = \frac{[\mathbf{B}^* \cdot \mathbf{B} + \mathbf{E}^* \cdot \partial(\omega \tilde{\epsilon})/\partial \omega \cdot \mathbf{E}]^{1/2}}{B_z}, \quad (1)$$

where all the field components are calculated from the cold plasma dispersion relation [4]. This factor depends only on the plasma density and the perpendicular wavelength. A gray scale is used in Fig. 2 to display the energy-scaled, normalized data with black representing the most negative values (i.e., wave troughs) and white representing the most positive values (i.e., wave crests). Superimposed, as a white line, on each picture is a density contour representing the edges of the striation.

The left picture of Fig. 2 clearly shows the incident whistler wave on the positive x side of the striation ($-9 \text{ cm} \leq x \leq 0 \text{ cm}$). The parallel wavelength is approximately 18 cm. As time advances, this pattern moves in the positive z direction constrained by the edge of the striation (normally the whistler radiation pattern spreads out in a cone). Also, the wave amplitude is peaked at the striation edge starting from $z \approx 30 \text{ cm}$ [see the amplitude profile in Fig. 2(a) which shows $|\tilde{B}_z(x)|^2$ at $z \approx 32 \text{ cm}$]. Inside the striation the wave amplitude drops off exponentially since the density inside is too low to support the whistler mode at the given parallel wavelength. After filtering out the long perpendicular wavelengths, lower hybrid waves can clearly be seen in Fig. 2(c). They have a perpendicular wavelength $\lambda_{\perp,LH}$ of about 1.5 cm. We further observe that they propagate toward the striation boundary as expected for these so-called “backward-propagating” waves (backward in the perpendicular direction). The amplitude of the lower hybrid waves is $\sim 20\%$ of the incident whistler wave amplitude. This implies that the energy density in lower hybrid waves is about 4% of the incident whistler wave energy density. The rest of the wave energy can be accounted for in the reflected whistler wave, transmitted lower hybrid wave, and in whistler radiation that refracts around and through the striation. It is important to point out that the same experiment had been carried out previously in a uniform plasma and that no short-wavelength waves were detected. Both the spatial pattern and the spectral characteristics match those predicted by the Green’s function analysis, mentioned above, containing only whistler wave modes.

The spatial distribution of the lower hybrid waves is as follows. The largest amplitude lower hybrid waves are on the incident wave side of the striation; there is only weak lower hybrid wave activity inside the striation and almost nothing on the far side. The large amplitude lower hybrid waves extend from the striation edge to the limit of the measurement region—a distance of about five perpendicular wavelengths. Interestingly, in a region extending two perpendicular wavelengths from the striation for $z < 30 \text{ cm}$ there is almost no lower hybrid wave activity. Recall that the axial position $z \approx 30 \text{ cm}$ is where the incident wave amplitude begins to show a peak at the striation boundary.

We also carried out a detailed Fourier analysis of these data. Since the data are in the form of a two-dimensional array, it is possible to perform a two-dimensional Fourier transform; however, the spectral peaks obtained from our data using this method are quite broad. In order to obtain more precise values of the k_{\parallel} and k_{\perp} peak values, we take the Fourier transform of each row (which is a function of z) to obtain its k_{\parallel} spectrum, and, conversely, the Fourier transform of each column (a function of x) to obtain the k_{\perp} spectrum. From the unfiltered data, we obtain the k_{\parallel} spectra of all data rows containing waves of significant amplitude and measure the k_{\parallel} of the peak of each spectrum. The range of these k_{\parallel} values is denoted by the horizontal gray band in Fig. 3. In the perpendicular direction, the dominant k_{\perp} of the unfiltered data ranges from $k_{\perp,W} = 0.7$ to 0.9 cm^{-1} , slightly narrower than the expected range for the long-wavelength incident whistler waves given the range of k_{\parallel} . The $k_{\perp,W}$ range is indicated by the left vertical gray band. After filtering out this range of dominant, long-wavelength $k_{\perp,W}$ values from the data, we find a smaller $k_{\perp,LH}$ peak remains in each k_{\perp} spectrum. The range of these $k_{\perp,LH}$ values is denoted by the right vertical gray band. We see that the intersection of the k_{\parallel} and $k_{\perp,LH}$ ranges is spanned by the dispersion curve.

This last result shows that the wavelength of lower hybrid waves generated by the interaction of whistler waves with a density striation is consistent with linear mode coupling. Also, the spatial pattern of the lower hybrid waves inside the striation and those outside the striation that are within $(2-3)\lambda_{\perp,LH}$ of the boundary (for $z > 30 \text{ cm}$) conform to what one would expect for

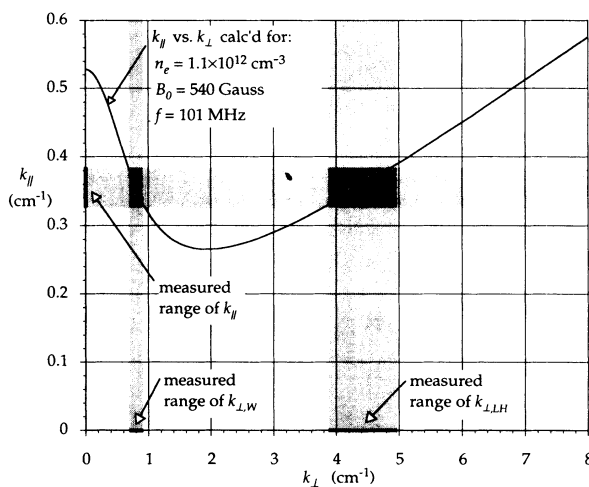


FIG. 3. k_{\parallel} vs k_{\perp} dispersion curve for the experimental parameters with measured ranges of incident k_{\parallel} values, incident whistler wave $k_{\perp,W}$ values, and mode-converted lower hybrid wave $k_{\perp,LH}$ values indicated with gray bands. The intersection of these ranges is spanned by the dispersion curve, as indicated by the heavier line sections, in agreement with the linear mode-coupling model.

the reflected and transmitted waves of an incident wave striking the boundary at $z \approx 30$ cm. However, the origin of the waves which are $(4-5)\lambda_{\perp, LH}$ from the boundary is less clear. We suspect that these arise as a result of whistler wave radiation impinging upon the entire length of the striation, due to reflection at the grid anode located at $z = -450$ cm (note that the antenna launches whistler waves symmetrically, both in the positive and negative z directions). Of course, some differences between our results and the predictions of the planar interface model are to be expected, because the striation is cylindrical, not planar. Further, the striation diameter is less than the whistler perpendicular wavelength and its density gradient scale length is approximately equal to the wavelength of the lower hybrid wave so that the density transition is not discontinuous as in the model. To our knowledge, there has been no theoretical treatment of this more complicated situation.

Of further significance, we would like to comment on the efficiency of the mode-conversion process. Above we reported that the energy density of the lower hybrid wave was about 4% of the incident whistler wave. If all of the whistler wave energy mode converted to the lower hybrid wave, the lower hybrid energy density would actually be much higher than 100% of the incident because the group velocity of the lower hybrid wave is

much slower than that of the whistler. On the other hand, in regions of the ionosphere where whistler waves are interacting with density striations, even 4% of the whistler wave energy density (20% of input amplitude) may produce significant short-wavelength electric fields. A more complete understanding of the mode-conversion efficiency as a function of the ratio of whistler wavelength to striation diameter and other plasma parameters awaits a thorough analysis of the other cases we have investigated. This and a full discussion of other features observed in the interaction, not explained by the linear mode-coupling model, will be presented in a future publication.

We would like to acknowledge the stalwart efforts of A. Burke, S. Rosenberg, T. Tisdale, and S. Vincena in acquiring the data. This research was supported by ONR Grant No. N0001491J1172.

-
- [1] T.F. Bell and H.D. Ngo, *J. Geophys. Res.* **93**, 2599 (1988).
 - [2] D.H. Clark and W.J. Raitt, *Planet Space Sci.* **24**, 873 (1976).
 - [3] W. Gekelman *et al.*, *Rev. Sci. Instrum.* **62**, 2875 (1991).
 - [4] Derived from T.H. Stix, *Waves in Plasmas* (McGraw-Hill, New York, 1992), p. 75, Eq. (20).

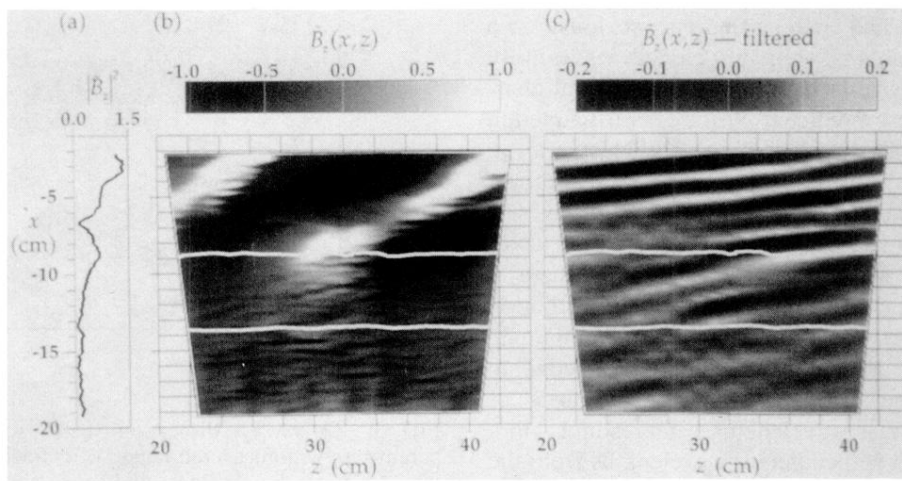


FIG. 2. Energy-scaled, normalized magnetic field data \tilde{B}_z plotted as a function of x and z with lines indicating the striation edges superimposed in (b) and (c). Whistler waves are clearly seen in the unfiltered data (b); lower hybrid waves are revealed by filtering the long perpendicular wavelengths from the data in (c). An amplitude profile of the unfiltered data at $z \approx 32$ cm appears in (a), showing a peak at the edge of the striation.

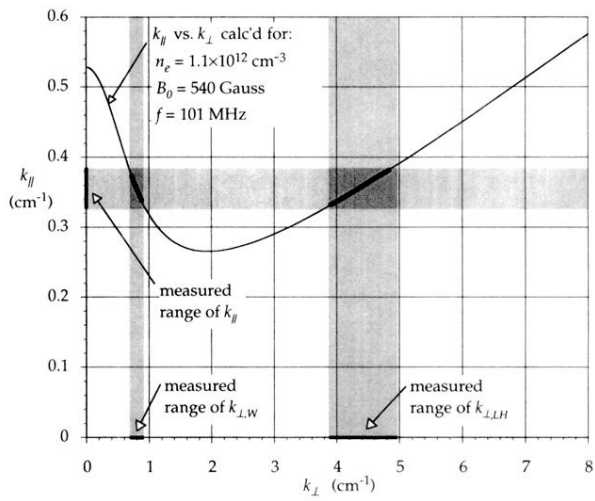


FIG. 3. k_{\parallel} vs k_{\perp} dispersion curve for the experimental parameters with measured ranges of incident k_{\parallel} values, incident whistler wave $k_{\perp,W}$ values, and mode-converted lower hybrid wave $k_{\perp,LH}$ values indicated with gray bands. The intersection of these ranges is spanned by the dispersion curve, as indicated by the heavier line sections, in agreement with the linear mode-coupling model.